Further Developments in Rapidly Decelerating Turbulent Pipe Flow Modeling

S. Meniconi[1], H.F. Duan[2], M. ASCE, B. Brunone[3], M. ASCE, M.S. Ghidaoui[4], P.J. Lee[5], M. ASCE, and M. Ferrante[6]

[1] Assistant Professor, Dipartimento di Ingegneria Civile e Ambientale, The University of Perugia, Via G. Duranti 93, 06125 Perugia, Italy. Email: silvia.meniconi@unipg.it.
[2] Assistant Professor, Department of Civil and Environmental Engineering, Hong Kong Polytechnic University, Hung Hom, Kowloon, Hong Kong.
Email: hf.duan@polyu.edu.hk. (*author for correspondence*)
[3] Professor, Dipartimento di Ingegneria Civile e Ambientale, The University of Perugia, Via G. Duranti 93, 06125 Perugia, Italy. Email: bruno.brunone@unipg.it.
[4] Chair Professor, Department of Civil and Environmental Engineering, The Hong Kong University of Science and Technology, Clear Water Bay, Kowloon, Hong Kong. Email: ghidaoui@ust.hk.
[5] Senior Lecturer, Department of Civil and Natural Resources Engineering, The University of Canterbury, Private Bag 4800 Christchurch, New Zealand. Email: pedro.lee@canterbury.ac.nz.
[6] Associate Professor, Dipartimento di Ingegneria Civile e Ambientale, The University of Perugia, Via G. Duranti 93, 06125 Perugia, Italy. Email: marco.ferrante@unipg.it.

Abstract: In the last two decades, energy dissipation in unsteady-state pressurized pipe flow has been examined by various authors, where the instantaneous wall shear stress is split into a quasi-steady and an unsteady shear stress component. The focus of most past studies is on formulating expressions for the unsteady wall shear stress, but there has been less work on the key parameters governing the dominance of unsteady friction in transient flows. This paper derives an expression for the head envelope damping for turbulent flows in smooth and rough pipes and provides new and carefully measured field data for the initial (i.e. pre-transient) Reynolds number, $\boldsymbol{Re_0}$, that ranges from 97000 to 380000. The analytical solution~~s~~ is derived on the basis of one-dimensional (1-D) waterhammer equations in which the unsteady component is represented by existing convolutional unsteady friction formulas for both smooth and rough turbulent sub-regimes. The analytical solution is used to formulate general, encompassing and theoretically-based dimensionless parameters to assess the importance of unsteady friction in comparison to the quasi-steady component. In addition, the analytical solution furnishes the similitude relations that allowed the damping behavior from existing laboratory tests, the field tests conducted as part of this research and the weighting function-based (WFB) models to be investigated and compared in a coherent manner in a single graph. The analysis confirms that the magnitude of $\boldsymbol{Re_0}$ has a significant impact on the damping for transients generated by flow stoppage. In addition, the results show that convolutional unsteady friction model that uses the frozen eddy viscosity hypothesis and Re_0 has accuracy that decreases with time. An improvement for this shortcoming is proposed and

verified and involves the use of the instantaneous Reynolds number in lieu of the pre-transient Reynolds number in the evaluation of the WFB models. The result is a modified unsteady friction model that provides improved matches for both laboratory and field data compared with the original model.

Authors Keywords: pressurized pipeline, turbulent flow, transients, unsteady friction, initial conditions, smooth pipe, rough pipe

Introduction

Various authors in the past two decades have examined energy dissiptation in unsteady-state pressurized pipe (waterhammer) flows. The convention in the waterhammer literature is to split the instantaneous wall shear stress, τ_w, into a sum of two components as follows,

$$\tau_w = \tau_{ws} + \tau_{wu} , \qquad (1)$$

where $\tau_{ws} = f \dfrac{\rho V |V|}{8}$ is the quasi-steady component with V, ρ and f being the instantaneous mean flow velocity, fluid density and friction factor, respectively; and τ_{wu} = unsteady component. The formulation of τ_{wu} has been the topic of intense study and new innovative approaches are continually being proposed in the literature (He and Jackson, 2000; Axworthy *et al.* 2000, Zhao *et al.* 2007; He and Jackson, 2011; Storli and Nielsen, 2011a and 2011b, and Mitosek and Szymkiewicz, 2012). The proposed models can be broadly classified into instantaneous acceleration-based (IAB) models (Brunone *et al.* 1991, 1995, 2004, Bergant *et al*. 2001, Brunone and Golia 2008, and Pezzinga 2009) and weighting function-based (WFB) models (Zielke 1968, Trikha 1975, Vardy and Brown 1995, 1996, 2003, 2004, 2010, Vitkovský *et al.* 2006, and Zarzycki, 2000). An indepth review of these models is given in Ghidaoui *et al.* (2005).

A promising and popular type of physically-based unsteady friction model is based on the WFB relations derived in Vardy and Brown (1995, 1996, 2003) for smooth-pipe flows and in Vardy and Brown (2004) for rough pipe flows. These models involve the following limiting assumptions: (i) the eddy viscosity is frozen to an idealized radial distribution whose parameters are determined from the pre-transient flow conditions and (ii) the derivation of the weighting function assumes that the fluid is incompressible. Therefore, it is important to address the following questions: What is the range of validity of these models? How can they be improved? When are these models required? Such questions have not received the attention they deserve and only limited progress has been made towards answering them. For example, Ghidaoui *et al.* (2002), and Duan *et al.* (2010, 2012) used a heuristic approach to identify some key parameters that can determine the conditions under which unsteady friction in transient flows is important. However, the approach used to arrive at the flow parameters is heuristic and cannot distinguish between smooth and rough pipe turbulence. The validity of WFB models is judged on the basis of comparison between measured and computed head traces (e.g., Bergant et al. 2001, Ghidaoui and Mansour 2002, Stephens et al. 2005). However, the lack of theoretically derived similitude relations prevented (i) the investigation of transient damping from different experiments and how this damping compares with WFB in a general and consistent manner and (ii) the generation of knowledge needed to propose improvement to existing WFB models.

This paper theoretically derives an expression for the head envelope damping for turbulent flow in smooth and rough pipes and provides new and carefully measured field data. The analytical solution provides general, encompassing and theoretically-based dimensionless parameters, instead of the heuristically-based parameters in Ghidaoui *et al.* (2002) and Duan *et al.* (2012), which can be used to assess the importance of unsteady friction in comparison to the quasi-steady component. In addition, the analytical solution furnishes the similitude relations that allow the damping behavior from existing laboratory tests, the field tests conducted as part of this research and the WFB models to be investigated and compared in a coherent manner in a single graph. As a result of this investigation, an improvement to existing WFB models is proposed and tested.

Further experiments on the role of Initial Reynolds Number

Description of Laboratory and Field Experiments

Experimental results were obtained from two separate sources to provide a rigorous test of the unsteady friction damping across a wide range of Reynolds numbers. The laboratory results are retrieved from Adamkowski and Lewandowski (2006) where the testing pipe system is a single copper pipe with pipe length L = 98.11 m, D = 16.0 mm, and wall thickness e = 1.0 mm. The Reynolds number of initial steady-state ($\boldsymbol{Re}_0$, with $\boldsymbol{Re} = VD/\nu$ = Reynolds number, D = pipe diameter, ν = fluid kinematic viscosity, L = pipe length, and the subscript 0 indicating the initial conditions) varies from 5.7×10^3 to 1.6×10^4 and the wavespeed, a, is 1298.4 m/s. Three tests from Adamkowski and Lewandowski (2006) are used for this study and the parameters of these tests are shown in Table 1 as test cases no. 1 through 3, with the measured pressure head, H, time-history – hereafter referred to as *pressure signal* – plotted in Figs. 1 though 3, where t indicates time since valve closure. The initial steady-state conditions of these three tests are smooth pipe flows.

Field tests were executed in the steel rising main connecting the Vallememoria well-field and the SAB reservoir in Recanati, Italy, managed by ASTEA spa. The steel pipe has D = 260 mm, L = 4170 m, and a = 1210 m/s and is supplied by three pumps installed in parallel. The static head, H_s, is 260 m and a check valve is installed immediately downstream of the pumping group. Note that all surge protection devices on the pipeline were deactivated. The parameters of the field tests are shown in Table 1 as test cases no. 4 through 7. The tests with the higher value of $\boldsymbol{Re}_0$ were previously presented in Brunone *et al.* (2001, 2002). Steady-state flow tests provided an estimate of the roughness height as ε = 2.2 mm. The initial steady-state flow conditions of all the field tests in Table 1 are in the fully rough pipe flow regime.

The pressure signal was measured immediately downstream of the check valve by a strain gauge pressure transducer with a recording range up to 400 m, an accuracy of ± 2 m and response time of 50 ms. The steady-state discharge was measured by a magnetic flowmeter just upstream of the check valve. The transient signals from a pump trip and the subsequent slamming of the check valve are shown in Figs. 4 through 7.

[add **Table 1** & **Figure 1** at this place]

Analysis of the induced damping of pressure oscillations

The crucial role of the Reynolds number for characterising uniform pipe flow emerged more than a century ago between laminar and turbulent regimes. The laminar regime, which exists for small values of $\boldsymbol{Re}$, is analytically tractable and governed by the well-known Hagen-Poiseouille relationship – in which the uniform wall shear stress, τ_w, is a function of V. On the contrary, the turbulent regime is ungovernable by any analytical model and then friction is evaluated by a myriad of empirical friction formulas where τ_w is a function of V^n, with $1.75 \leq n \leq 2$ according to the turbulent subregime.

For the case of highly unsteady pipe flow, the first work that investigated the role of $\boldsymbol{Re}_0$, is by Holmboe and Rouleau (1967). They considered the case of unsteady pipe flow induced by a complete and fast closure of a valve placed at the downstream end of a single pipe (i.e., constant diameter and supply head). They reported that when the initial flow was unquestionably laminar, a noticeable distortion and damping of the pressure, H, occurred after the first half transient cycle. On the contrary, for larger values of $\boldsymbol{Re_0}$, the experimental pressure signals were quite similar to those given by the frictionless Allievi-Joukowsky theory. In Vardy and Brown (2003, 2004) the influence of $\boldsymbol{Re_0}$ on the value of the unsteady friction coefficient has been pointed out for both smooth and rough pipe flow. Recently, Duan et al. (2012) has examined this problem more systematically by means of a simplified analytical model for smooth pipe, but their results have only been validated in a limited range of $\boldsymbol{Re}_0$ by the experimental data from the literature.

In this section, numerical simulation is first applied to all the test cases to investigate the importance of unsteady friction as a function of $\boldsymbol{Re}_0$ to further verify the results obtained in Duan et al. (2012) in a larger number of flow conditions. A 1-D method of characteristics model is used where only the effect of quasi-steady friction is considered (Ghidaoui et al. 2005). The differences between the experiments and the model provide an indicative magnitude of the omitted unsteady friction effect in the experiments. The time traces between the numerical model and the experiments are compared in Figs. 1, 2, and 3 for the laboratory tests and in Figs. 4, 5, 6, and 7 for the field tests. In these figures the results from the numerical model is labeled as “H_n” and experimental data is labelled as “H_e”. It is also worth noting that the transient head for laboratory test cases no. 1 through 3 is defined by the difference between the total pressure head at the valve and the steady-state head at the upstream reservoir (constant head), so that after normalization the initially transient head response in Figs. 1 to 3 is smaller than 1. This definition of the transient head is consistent with the original publication by Adamkowski and Lewandowski (2006). The results show that the match between the model and the experiments improves with increasing $\boldsymbol{Re}_0$, which indicates that the importance of unsteady friction is decreasing with Reynolds number. This result is confirmed by the values of the determination coefficient, R^2, which denotes the strength of the linear association between the experimental head response and the predicted head response from the quasi-steady 1-D model. The determination coefficient is defined as,

$$R^2 = 1 - \frac{SS_{err}}{SS_{tot}} = 1 - \frac{\sum_i \left(y_i^e - y_i^n\right)^2}{\sum_i \left(y_i^e - \overline{y_i^e}\right)^2} \tag{2}$$

where SS_{err} = sum of squares of residuals, and SS_{tot} = total sum of squares (proportional to the sample variance), y_i^e = experimental value (with the overbar indicating the mean value), and y_i^n = numerical model value. A R^2 value closer to unity represents a more accurate model prediction. The results of R^2 for all test cases in Table 1 are shown in Fig. 8. The trend of the determination coefficient in Fig. 8 is consistent with the results in Duan *et al.* (2012), which conclude that the importance of unsteady friction decreases with system scale and $\boldsymbol{Re}_0$.

[add **Figures 1 ~ 8** at this place]

Further insight into the behavior of the unsteady friction model can be found by deriving the envelope of the downstream pressure head and velocity oscillations for a single pipe where the downstream boundary valve is suddenly shut. The head and flow envelopes are given as follows (see derivation in Appendix I):

$$H_{amp}(t) = \frac{aV_0}{g} e^{-K_{r0}\frac{t}{T_w}} = \frac{aV_0}{g} e^{-K_{rs0}\frac{t}{T_w}} e^{-K_{ru0}\frac{t}{T_w}} = \frac{aV_0}{g} e^{-K_{rs0}\left(1+\frac{K_{ru0}}{K_{rs0}}\right)\frac{t}{T_w}}, \qquad (3)$$

and

$$V_{amp}(t) = V_0 e^{-K_{r0}\frac{t}{T_w}} = V_0 e^{-K_{rs0}\frac{t}{T_w}} e^{-K_{ru0}\frac{t}{T_w}} = V_0 e^{-K_{rs0}\left(1+\frac{K_{ru0}}{K_{rs0}}\right)\frac{t}{T_w}}, \qquad (4)$$

where subscript "*amp*" denotes amplitude, g = gravitational acceleration, K_{ru0} = damping rate due to unsteady friction, K_{rs0} = damping rate due to steady friction, $K_{r0}=K_{ru0}+K_{rs0}$ = total damping rate, and $T_w = L/a$ is wave timescale. The expressions of K_{r0}, K_{ru0}, and K_{rs0} for smooth pipe flow have been derived using the unsteady friction weighting functions of Vardy and Brown (1995, 1996, and 2003) in Duan *et al.* (2012). The parameters for fully rough pipe flow are derived using the unsteady friction model of Vardy and Brown (2004) in the present study (see Eqs. A22 and A23 in Appendix I).

According to Eqs. (3) and (4), the ratio K_{ru0}/K_{rs0} provides a measure for the relative importance of unsteady friction to steady friction. In particular, it is clear from the analytical solution that unsteady friction is not important when K_{ru0}/K_{rs0}<<1 and important otherwise. The expression for this ratio is given as below,

(i) for smooth pipe flow case:

$$\frac{K_{ru0}}{K_{rs0}} = \begin{cases} \dfrac{2\sqrt{2}}{f\boldsymbol{Re}_0}\sqrt{\dfrac{T_{dv}}{T_w}} & if\ \boldsymbol{Re}_0 \dfrac{T_w}{T_{dv}} << 1 \\ \dfrac{0.066}{f\left(\boldsymbol{Re}_0\right)^{1.94}}\left(\dfrac{T_{dv}}{T_w}\right)^2 & \text{otherwise} \end{cases} = \begin{cases} \dfrac{2\sqrt{2}}{f\sqrt{\boldsymbol{M}\boldsymbol{Re}_0}}\sqrt{\dfrac{D}{L}} & if\ \boldsymbol{M}\dfrac{L}{D} << 1 \\ \dfrac{0.066}{f\left(\boldsymbol{Re}_0\right)^{-0.06}\boldsymbol{M}^2}\left(\dfrac{D}{L}\right)^2 & \text{otherwise} \end{cases}; \qquad (5)$$

(ii) for rough pipe flow case:

$$\frac{K_{ru0}}{K_{rs0}} = 0.048\left(\frac{\varepsilon}{D}\right)^{0.016}\left(\frac{T_{dv}}{T_w}\right)^{1.414}\frac{1}{f\boldsymbol{Re}_0^{1.414}} = 0.048\left(\frac{\varepsilon}{D}\right)^{0.016}\left(\frac{D}{L}\right)^{1.414}\frac{1}{f\boldsymbol{M}^{1.414}}\,. \tag{6}$$

where $T_{dv} = D^2/\nu$ is viscous diffusion timescale.

It is clear from Eqs. (5) and (6) that the relative importance of the unsteady and quasi-steady components depends on (i) the pre-transient Reynolds number $\boldsymbol{Re}_0$, timescale ratio T_w/T_{dv}, Mach number $\boldsymbol{M}$ and L/D for smooth turbulent flows and (ii) $\boldsymbol{Re}_0$, T_w/T_{dv}, $\boldsymbol{M}$, L/D and relative roughness ε/D for rough turbulent flows. Both Eqs. (5) and (6) support the finding of the last section in that $K_{ru0}/K_{rs0} \ll 1$ as $\boldsymbol{Re}_0$ gets larger.

Table 1 provides the relevant parameters for the different test cases. The K_{ru0}/K_{rs0} column shows that the condition $K_{ru0}/K_{rs0} \ll 1$ is indeed valid for the test rigs for which the unsteady component is deemed irrelevant and K_{ru0}/K_{rs0} is of order 1 for the test rigs for which the unsteady component is deemed important. For example, $K_{ru0}/K_{rs0} = 1.19$ for case 1 which implies that the quasi-steady and unsteady component are of the similar importance and explains why the model which neglects the unsteady friction component provides poor agreement with the data as reported in Figure 1. In addition, both the analytical solution and Table 1 clearly show that the importance of unsteady friction diminishes with $\boldsymbol{Re}_0$. Moreover, the table also indicates the consistency between the values of the K_{ru0}/K_{rs0} column and the parameter $\boldsymbol{I}$ column, where $\boldsymbol{I} = f\boldsymbol{Re}_0 T_w/T_{dv} = f\boldsymbol{M}L/D$ as presented in Duan *et al.* (2012), where unsteady friction is deemed unimportant as $\boldsymbol{I}$ gets larger.

Validity of Frozen Turbulence Hypothesis and Proposed Improvement to Existing WFB Models

The fact that the analytical solution of the pressure head damping presented in the previous section is only a function of $\boldsymbol{Re}_0$ and not a time-dependent Reynolds number is largely an artifact of the frozen turbulence hypothesis used in the derivation of the friction model in Vardy and Brown (1995, 1996, 2003 and 2004). The ramifications of the frozen turbulence hypothesis are investigated below.

The damping from unsteady friction can be more elegantly represented by rewriting the pressure head envelope (H_{amp}) equation in Eq. (3) as follows:

$$\frac{1}{-K_{r0}}\ln\frac{gH_{amp}(t)}{aV_0} = \frac{t}{T_w}\,, \tag{7}$$

which shows that the pressure head envelope of all transient events, provided that the WFB unsteady friction model is valid, should collapse onto one single line. To test the validity of equation and by implication the validity of the frozen turbulence hypothesis, the variations of rescaled pressure envelope with respect to time for all seven cases are plotted in Fig. 9. The peak magnitude within each period of oscillation is used as H_{amp} in the figures. Furthermore, the scaled pressure envelopes predicted by the Vardy and Brown (1995, 1996 and 2003) for smooth pipe turbulent flow and Vardy and Brown (2004) for rough pipe turbulent flows for each test are also shown on the graphs. It is clear from the figure that in the early stages of the transient: (i) the scaled peak pressure envelope from the experiments varies linearly with time and (ii) the seven scenarios neatly collapse into a single line. This result indicates that the damping model is valid within the early stages of the transient. This conclusion is consistent with the previous results in Table 1 where the comparative plots of numerical and experimental data showed the prediction of the damping envelope decreases in accuracy with simulation time for current $\boldsymbol{Re}_0$ based unsteady friction models—which encompasses the IAB model by Brunone *et al.* (1991, 1995) and the WFB models by Vardy and Brown (1996, 2003) and Zarzyki (2000). In other words, the frozen turbulence assumption based on the $\boldsymbol{Re}_0$ condition adopted in these unsteady friction models is most valid in the early stage of the transient and becomes progressively poor as time advances.

[add **Figure 9** at this place]

The result in Fig. 9 shows that while the scaled pressure envelopes converge into a single line in the early stages of the transient, they diverge and become non-linear as the transient proceeds. Such a departure from linearity and the loss of self similarity for large time indicates that the predicted damping from the WFB unsteady friction model, which is based on the assumption of frozen initial turbulence, begins to lose its accuracy at the later stages of the transient. For a valve closure event, the mean flow velocity and turbulent structure are expected to decay with time as the system oscillates towards a new mean state (He and Jackson 2000, Ghidaoui *et al.* 2002). During the transient event, the turbulent viscosity distribution and the thickness of the shear layer will change and the flow will progressively lose dependence on $\boldsymbol{Re}_0$. While the frozen turbulent flow hypothesis is valid for the early stages of the transient event (Ghidaoui *et al.* 2002), this assumption becomes progressively violated at later stages.

Experimental investigation of turbulence behavior in transient flows in pipes (e.g., He and Jackson 2000, He *et al.* 2011, and Vardy and Brown 2010) reported that the instantaneous and not the pre-transient Reynolds number is the appropriate parameter that collapses turbulent fluctuations and wall shear stress from different experiments into single curves. Using the instantaneous velocity amplitude instead of V_0 to define the local Reynolds number, $\boldsymbol{Re}_t$, as follows:

$$\boldsymbol{Re}_t = \frac{V_{amp}(t)D}{\nu} = \frac{\left(V_0 e^{-K_{r0}\frac{t}{T_w}}\right)D}{\nu} = \boldsymbol{Re}_0 e^{-K_{r0}\frac{t}{T_w}} \tag{8}$$

and re-defining the total damping rate in terms of the local Reynolds number by inserting $\boldsymbol{Re}_t$ in place of $\boldsymbol{Re}_0$ in Eqs. (A23) and (A22) respectively, gives:

(i) for smooth pipe flow case:

$$K_r(t) \approx \begin{cases} \dfrac{f\boldsymbol{Re}_t}{2}\dfrac{T_w}{T_{dv}} + \sqrt{2\dfrac{T_w}{T_{dv}}} & \text{if } \boldsymbol{Re}_0 \dfrac{T_w}{T_{dv}} << 1 \\ \dfrac{f\boldsymbol{Re}_t}{2}\dfrac{T_w}{T_{dv}} + \dfrac{1}{30.33\left(\boldsymbol{Re}_t\right)^{0.94}}\dfrac{T_{dv}}{T_w} & \text{otherwise} \end{cases}$$
$$= \begin{cases} \dfrac{f\boldsymbol{Re}_0 e^{-K_{r0}\frac{t}{T_w}}}{2}\dfrac{T_w}{T_{dv}} + \sqrt{2\dfrac{T_w}{T_{dv}}} & \text{if } \boldsymbol{Re}_0 \dfrac{T_w}{T_{dv}} << 1 \\ \dfrac{f\boldsymbol{Re}_0 e^{-K_{r0}\frac{t}{T_w}}}{2}\dfrac{T_w}{T_{dv}} + \dfrac{1}{30.33\left(\boldsymbol{Re}_0 e^{-K_{r0}\frac{t}{T_w}}\right)^{0.94}}\dfrac{T_{dv}}{T_w} & \text{otherwise} \end{cases}; \tag{9}$$

(ii) for rough pipe flow case:

$$K_r(t) \approx \frac{f\boldsymbol{Re}_t}{2}\frac{T_w}{T_{dv}} + 0.024\left(\frac{\varepsilon}{D}\right)^{0.016}\left(\boldsymbol{Re}_t \frac{T_w}{T_{dv}}\right)^{-0.414}$$
$$= \frac{f\boldsymbol{Re}_0 e^{-K_{r0}\frac{t}{T_w}}}{2}\frac{T_w}{T_{dv}} + 0.024\left(\frac{\varepsilon}{D}\right)^{0.016}\left(\boldsymbol{Re}_0 e^{-K_{r0}\frac{t}{T_w}}\frac{T_w}{T_{dv}}\right)^{-0.414}. \tag{10}$$

To judge the appropriateness of the proposed re-scaling, the re-scaled amplitude $\dfrac{1}{-K_r(t)}\ln\dfrac{gH_{amp}(t)}{aV_0}$ versus time and with $K_r(t)$ given by Eq. (9) or (10) is plotted in Fig. 10. The data from all seven cases now neatly collapses into a single linear curve. This collapse provides strong support for the fact that turbulent conditions within real transient flows are not frozen but change with the transient duration and that a relaxation of this assumption allows better match with the model at all times. As a consequence, it is proposed that the instantaneous, rather than the initial, Reynolds number is used in convolution integrals unsteady friction formulas for turbulent flows. The Vardy and Brown convolutional unsteady friction model is modified accordingly and then implemented into a 1-D waterhammer model. The modified and original model are then applied and compared to the laboratory (case no. 3

in Table 1) and field data (case no. 6 in Table 1) and the results are shown in Figs. 11 and 12, respectively. These cases are chosen because they are the ones for which the frozen turbulence hypothesis is the least valid.

[add **Figures 10~12** at this place]

Figures 11 and 12 clearly show the gradual departure of the pressure head envelope (peaks) by the original model from the experimental data. On the other hand, the results of modified model are in better agreement with the experimental data throughout the entire simulation time. Moreover, greater improvement resulted for the larger $\boldsymbol{Re}_0$ case which represents a practical field system application.

Conclusions

Many papers in recent years have focused on methods for estimating the unsteady shear stress in transient flows and a popular type of physically-based unsteady friction model uses the WFB relations derived in Vardy and Brown (1995, 1996, 2003) for smooth-pipe flows and in Vardy and Brown (2004) for rough pipe flows. Despite the number of studies in this area, no rigorous similitude analysis has been conducted on the model to (i) allow meaningful comparisons of unsteady friction damping on transient responses of different pipeline systems (ii) provide insight into the key parameters driving the damping of the head envelope and (iii) identify limitations in the current model.

This paper theoretically derives an expression for the head envelope damping for turbulent flow in smooth and rough pipes and provides general, encompassing and theoretically-based dimensionless parameters, instead of the heuristically-based parameters in Ghidaoui et al (2002) and Duan et al. (2012), that can be used to assess the importance of unsteady friction in comparison to the quasi-steady component. The dimensionless parameters allow~~s~~ the damping behavior from existing laboratory tests, the field tests conducted as part of this research and the WFB models to be investigated and compared in a coherent manner in a single graph. The key findings are as follows:

(1) The general trend that the importance of unsteady friction in rapidly decelerating flows diminishes with $\boldsymbol{Re}_0$ has been extended and validated for a larger number of initial conditions.

(2) The accuracy of existing convolutional unsteady friction model, which are based on the frozen eddy viscosity hypothesis such that the resulting convolution integrals are a

function of the pre-transient and not a time dependent Reynolds number, decreases with simulation time of wave propagation.

(3) An improvement for the shortcoming in (2) is proposed and verified. It involves the use of the instantaneous Reynolds number ($\boldsymbol{Re_t}$) in lieu of the pre-transient Reynolds number ($\boldsymbol{Re}_0$) in the evaluation of the convolution integral models. The result indicates that the modified unsteady friction model agrees better with data than the original model. The use of $\boldsymbol{Re_t}$ is inspired by previous experimental investigation of turbulence behavior in transient flows in pipes which show that the instantaneous and not the pre-transient Reynolds number is the appropriate parameter for scaling turbulent fluctuations and wall shear stress.

Acknowledgements:

This research has been supported by: (i) Italian Ministry of Education, University and Research under the Projects of Relevant National Interest "Advanced analysis tools for the management of water losses in urban aqueducts", and "Tools and procedures for an advanced and sustainable management of water distribution systems"; (ii) the Hong Kong Research Grant Council under the projects nos. 612511 and 612910; and (iii) the Royal Society of New Zealand with Marsden Grant UOC1153.

References

Adamkowski, A., and Lewandowski, M. (2006). Experimental examination of unsteady friction models for transient pipe flow simulation. *Journal of Fluids Engineering*, ASME, 128(6), pp. 1351-1363.

Axworthy, DH, Ghidaoui, MS, and McInnis, DA. (2000). Extended thermodynamics derivation of energy dissipation in unsteady pipe flow. *Journal of Hydraulic Engineering,* ASCE, 126(4), pp. 276-287.

Bergant, A, Simpson, AR, and Vitkovsky, J. (2001). Developments in unsteady pipe flow friction modelling. *Journal of Hydraulic Research,* IAHR, 39(3), pp. 249-257.

Brunone, B., Golia, U. M., and Greco, M. (1991). Some remarks on the momentum equations for fast transients. In Cabrera, E. and Fanelli, M., editors, *Proc. "International Meeting on Hydraulic Transients with Column Separation"*, *9th Round Table*, IAHR, Valencia (E), pp. 140-148.

Brunone, B., Golia, U.M., and Greco, M. (1995). Effects of two-dimensionality on pipe transients modelling. *Journal of Hydraulic Engineering,* ASCE, 121(12), pp. 906-912.

Brunone, B., Ferrante, M., and Calabresi, F. (2001). High Reynolds number transients in a pump rising main. Field tests and numerical modeling. In Lowdon, A., editor, *Proc., 4th Int. Conference "Water Pipeline Systems"*, York (UK), BHR Group, pp. 339-348.

Brunone, B., Ferrante, M., and Calabresi, F. (2002). Discussion of "Evaluation of unsteady flow resistances by quasi-2D or 1D models", by G. Pezzinga. *Journal of Hydraulic Engineering,* ASCE, 128(6), pp. 646-647.

Brunone, B., Ferrante, M., and Cacciamani, M. (2004). Decay of pressure and energy dissipation in laminar transient flow. *J. of Fluids Engineering*, ASME, 126(6), pp. 928-934.

Brunone, B., and Golia, U.M. (2008). Discussion of "Systematic evaluation of one-dimensional unsteady friction models in simple pipelines" by J.P. Vitkovsky, A. Bergant, A.R. Simpson, and M. F. Lambert. *J. of Hydraulic Engineering*, ASCE, 134(2), pp. 282-284.

Duan, H.F., Ghidaoui, M.S., Lee, P.J. and Tung, Y.K. (2010). Unsteady friction and visco-elasticity in pipe fluid transients. *Journal of Hydraulic Research*, IAHR, 48(3), pp. 354-362.

Duan, H.F., Ghidaoui, M.S. Lee, P J and Tung, Y K. (2012). Relevance of unsteady friction to pipe size and length in pipe fluid transients. *Journal of Hydraulic Engineering,* ASCE, 138(2), pp. 154-166.

Ghidaoui, MS, Mansour, SGS, and Zhao, M. (2002). Applicability of quasisteady and axisymmetric turbulence models in water hammer. *Journal of Hydraulic Engineering,* ASCE, 128(10), pp. 917-924.

Ghidaoui, M.S. and Mansour, S. (2002). Efficient Treatment of the Vardy-Brown Unsteady Shear in Pipe Transients. *Journal of Hydraulic Engineering,* ASCE, 128(1), pp. 102-112.

Ghidaoui, MS, Zhao, M., McInnis, DA, and Axworthy, DH. (2005). A review of water hammer theory and practice. *Applied Mechanics Reviews*, 58(1), pp. 49-76.

He, S., and Jackson, J. D. (2000). A study of turbulence under conditions of transient flow in a pipe. *Journal of Fluid Mechanics*, 408, pp. 1-38.

He, S., Ariyaratne, C. and Vardy, A.E. (2011). Wall shear stress in accelerating turbulent pipe flow. *Journal of Fluid Mechanics*, 685, pp. 440-460.

Holmboe, EL, and Rouleau, WT. (1967). The effect of viscous shear on transients in liquid lines. *Journal of Basic Engineering,* ASME, 89(1), pp. 174-180.

Mitosek, M., and Szymkiewicz, R. (2012). Wave damping and smoothing in the unsteady pipe flow. *Journal of Hydraulic Engineering*, ASCE, 138(7), pp. 619-628.

Pezzinga, G. (2009). Local balance unsteady friction model. *Journal of Hydraulic*

Engineering, ASCE, 135(1), pp. 45-56.

Silva-Araya, WF, and Chaudhry, MH. (2001). Unsteady friction in rough pipes. *Journal of Hydraulic Engineering,* ASCE, 127(7), pp. 607-618.

Silva-Araya, WF, and Chaudhry, MH. (1997). Computation of energy dissipation in transient flow. *Journal of Hydraulic Engineering,* ASCE, 123(2), pp. 108-115.

Stephens M., Simpson A. R., Lambert M. F., and Vítkovsky J. P. (2005). Field measurement of unsteady friction effects in a trunk transmission pipeline. *Proc. Int. Conf. of 7th Annual Symposium on Water Distribution Systems Analysis*, Anchorage, Alaska, USA, 15-19 May, 2005.

Storli, P-T, and Nielsen, TK. (2011a). Transient friction in pressurized pipes. ii: two-coefficient instantaneous acceleration-based model. *Journal of Hydraulic Engineering,* ASCE, 137(6), pp. 679-695.

Storli, P-T, and Nielsen, TK. (2011b). Transient friction in pressurized pipes III: investigation of the EIT model based on position-dependent coefficient approach in MIAB model. *Journal of Hydraulic Engineering,* ASCE, 137(9), pp. 1047-1053.

Trikha, AK. (1975). An efficient method for simulating frequency-dependent friction in transient liquid flow. *Journal of Fluids Engineering,* ASME, 97(1), pp. 97-105.

Vardy, AE and Brown, JMB. (1995). Transient, turbulent, smooth pipe friction. *Journal of Hydraulic Research, IAHR*, 33(4), pp. 435-456.

Vardy, AE and Brown, JMB. (1996). On turbulent, unsteady, smooth-pipe friction. *Proc., 7th Int. Conf. on "Pressure Surges and Fluid Transients in Pipelines and Open Channels"*, Harrogate (UK), BHR Group, pp. 289-311.

Vardy, AE and Brown, JMB. (2003). Transient turbulent friction in smooth pipe flows. *Journal of Sound and Vibration*, 259(5), pp. 1011-1036.

Vardy, AE and Brown, JMB. (2004). Transient turbulent friction in fully rough pipe flows. *Journal of Sound and Vibration*, 270(2), pp. 233-257.

Vardy, AE, and Brown, JMB. (2010). Influence of time-dependent viscosity on wall shear stresses in unsteady pipe flows. *Journal of Hydraulic Research,* IAHR, 48(2), pp. 225-237.

Vitkovský, J., Stephens, M., Bergant, A., Simpson, A., and Lambert, M. (2006). Numerical error in weighting function-based unsteady friction models for pipe transients. *Journal of Hydraulic Engineering,* ASCE, 132(7), pp. 709-721.

Zarzycki, Z. (2000). On weighting function for wall shear stress during unsteady turbulent pipe flow. *Proc., 8th Int. Conf. on Pressure Surges*, The Hague (NL), BHR Group, pp.

529-543.
Zhao, M., Ghidaoui, M.S., and Kolyshkin, A. A. (2007). Perturbation dynamics in unsteady pipe flows. *Journal of Fluid Mechanics*, 570, pp. 129-154.
Zielke, W. (1968). Frequency-dependent friction in transient pipe flow. *Journal of Basic Engineering*, ASME, 90(1), pp. 109-115.

Appendix I: Analytical Solution of Transient Oscillating Envelope

The 1-D waterhammer equations in the dimensionless form used for this study are (Ghidaoui *et al.* 2005, Duan *et al.* 2012):

$$\frac{\partial H^*}{\partial t^*}+\frac{aQ_0}{gAH_0}\frac{\partial Q^*}{\partial x^*}=0, \tag{A1}$$

$$\frac{\partial Q^*}{\partial t^*}+\frac{gAH_0}{aQ_0}\frac{\partial H^*}{\partial x^*}+\frac{fLQ_0}{aDA}Q^*+\frac{4\pi\nu L}{aA}\int_0^t W\left(t'^*\right)\frac{\partial Q^*}{\partial t'^*}dt'^*=0\ . \tag{A2}$$

where Q = flow discharge; x = the distance along pipeline; and t' is a dummy time variable; other symbols have been defined in the previous text; superscript "*" is representing dimensionless form, and the following dimensionless quantities are considered:

$$H^*=\frac{H}{H_0};\ Q^*=\frac{Q}{Q_0};\ t^*=\frac{t}{T_w};\ \text{and}\ x^*=\frac{x}{L}. \tag{A3}$$

As indicated in Eq. (1) in the text, the total shear stress (τ_w) in transients has been separated into two parts to isolate the impacts of quasi-steady and unsteady friction components in Eq. (A2) above: a quasi-steady part (τ_{ws}) and an unsteady part (τ_{wu}). Moreover, the quasi-steady part relating to the average velocity is represented by the classic Darcy-Weisbach equation (Ghidaoui *et al.* 2005), and for the possibility of analytical derivation, it has been linearized for relatively small transient flow as (Duan *et al.* 2012):

$$\tau_{ws}=\frac{\rho fQ^2}{4A^2}\approx\frac{\rho fQ_0}{4A^2}\left(Q_0+q\right)=\frac{\rho fQ_0}{4A^2}Q, \tag{A4}$$

where q is the oscillation of unsteady flow in pipeline relative to steady-state (pre-transient state), and $q = Q - Q_0$. Theoretically Eq. (A4) is derived for $q \ll Q_0$, however it has also been validated in Duan *et al.* (2012) by using 2-D numerical simulations that Eq. (A4) is also valid for the transients caused by the full closure of end valve.

On the other hand, the unsteady part is related to the fluid acceleration by the convolution integral relations (i.e., WFB models) such as the one in Zielke (1968) for laminar flows and Vardy and Brown (1995, 1996, 2003, and 2004) for turbulent flows. The general form of this WFB model is:

$$\tau_{wu} = \frac{4\rho\nu}{DA}\int_0^t W(t-t')\frac{\partial Q(t')}{\partial t'}dt', \tag{A5}$$

For laminar flow regime, the weighting function can be expressed by exponential relations and details refer to Zielke (1968) or Ghidaoui *et al.* (2005). While for the turbulent case, an approximated expression of the weighting function in a dimensionless form has been derived by Vardy and Brown (1995, 1996, 2003, and 2004):

$$W(t^*) = \alpha' \frac{e^{-\beta' t^*}}{\sqrt{\pi t^*}}, \tag{A6}$$

where α', β' are coefficients relating to transient evens and the pipeline system under investigation. Specifically, for smooth pipe flows (Vardy and Brown 1995, 1996),

$$\alpha' = \frac{1}{4}\sqrt{\frac{T_{dv}}{T_w}}, \text{ and } \beta' = 0.54 k_{Re_0}\frac{T_w}{T_{dv}}, \tag{A7}$$

where $T_w = L/a$ is longitudinal wave timescale, $T_{dv} = D^2/\nu$ is radial viscous diffusion timescale, and $k_{Re_0} = (\boldsymbol{Re}_0)^{\log\left(14.3/(Re_0)^{0.05}\right)}$ is initial Reynolds number based coefficient.

For fully rough pipe flows (Vardy and Brown 2003, 2004), the coefficients are,

$$\alpha' = 0.00913\left(\frac{\varepsilon}{D}\right)^{0.39}\sqrt{\boldsymbol{Re}_0\frac{T_{dv}}{T_w}}, \text{ and } \beta' = 1.408\left(\frac{\varepsilon}{D}\right)^{0.41}\boldsymbol{Re}_0\frac{T_w}{T_{dv}}, \tag{A8}$$

To investigate the effect of different parameters of pipeline system and transient events on the friction (steady and unsteady) induced damping of the transient envelope, similar analytical analysis process can be conducted with the aid of applying Fourier transform to system Eqs. (A1) and (A2). The obtained results are,

$$i\omega^*\hat{H}^* + \frac{aQ_0}{gAH_0}\frac{\partial \hat{Q}^*}{\partial x^*} = 0, \tag{A9}$$

$$i\omega^*\hat{Q}^* + \frac{gAH_0}{aQ_0}\frac{\partial \hat{H}^*}{\partial x^*} + \frac{fLQ_0}{aDA}\hat{Q}^* + \frac{4\pi\nu L}{aA}\frac{i\alpha'\omega^*}{\sqrt{\beta' + i\omega^*}}\hat{Q}^* = 0, \tag{A10}$$

where $\hat{H}^*(x^*,\omega^*)$, $\hat{Q}^*(x^*,\omega^*)$ are the amplitudes of head and discharge in the frequency domain, ω^* is angular frequency of transient signals.

By combining Eqs. (A9) and (A10), the resultant equations for pressure head and discharge are,

$$\frac{\partial^2\hat{H}^*}{\partial(x^*)^2} + C^*\hat{H}^* = 0, \text{ and } \frac{\partial^2\hat{Q}^*}{\partial(x^*)^2} + C^*\hat{Q}^* = 0, \tag{A11}$$

where C^* is a lumped parameter for wave propagation, and,

$$C^* = \left(\omega^*\right)^2 \left(1 - i\frac{fLQ_0}{aDA\omega^*} + \frac{4\pi\nu L}{aA}\frac{\alpha'}{\sqrt{\beta' + i\omega^*}}\right). \tag{A12}$$

It is easy to obtain the form of the solution to Eq. (A11) given by (Duan *et al.* 2012),

$$\hat{H}^*\left(x^*, \omega^*\right) = \hat{H}_0^* e^{-K_0 x^*}, \text{ and } \hat{Q}^*\left(x^*, \omega^*\right) = \hat{Q}_0^* e^{-K_0 x^*}, \tag{A13}$$

where $\hat{H}_0^*$, $\hat{Q}_0^*$ relate to the initial values (head and discharge); and $K_0 = K_{r0} + iK_{i0}$ with K_{r0} and K_{i0} the parameters of the wave envelope decay and phase shift, respectively, and,

$$K_{r0} = \sqrt{\frac{\sqrt{(\Omega_1)^2 + (\Omega_2)^2} - \Omega_1}{2}}; \quad K_{i0} = \sqrt{\frac{\sqrt{(\Omega_1)^2 + (\Omega_2)^2} + \Omega_1}{2}}, \tag{A14}$$

where,

$$\Omega_1 = 1 + \frac{4\pi\nu L\alpha'}{aA}\sqrt{\frac{\sqrt{(\beta')^2 + (\omega^*)^2} + \beta'}{2\left((\beta')^2 + (\omega^*)^2\right)}}; \quad \Omega_2 = \frac{fLQ_0}{aDA\omega^*} + \frac{4\pi\nu L\alpha'}{aA}\sqrt{\frac{\sqrt{(\beta')^2 + (\omega^*)^2} - \beta'}{2\left((\beta')^2 + (\omega^*)^2\right)}}. \tag{A15}$$

Consequently, it is now clear from Eqs. (A13) through (A15) that the transient oscillation responses for pressure head and discharge are damping exponentially in the frequency domain. Meanwhile, in the single pipe the wave propagation period $T_w \sim L/a$ is corresponding to the distance of wave propagating cycles along the pipeline, i.e., $x^* \sim 1$ in the dimensionless form. Therefore the damping factor of the transient envelope for each wave period is approximated by e^{-K_0}. As a result for the n^{th} period (or n^{th} envelope location), the damped transient envelope becomes,

$$H_{amp}(n) = H_{amp0} e^{-nK_{r0}}, \text{ and } Q_{amp}(n) = Q_{amp0} e^{-nK_{r0}}, \tag{A16}$$

where subscript "*amp*" denotes amplitude, n is number of wave period, H_{amp0}, Q_{amp0} = quantities relating to initial (pre-transient) state conditions, and $H_{amp0} = \frac{aV_0}{g}$, $Q_{amp0} = Q_0$ for the transients caused by sudden valve closure and pump failure considered in this study. In terms of wave time, the result becomes,

$$H_{amp}(t) = \frac{aV_0}{g} e^{-K_{r0}\frac{t}{T_w}}, \text{ and } Q_{amp}(t) = Q_0 e^{-K_{r0}\frac{t}{T_w}}, \tag{A17}$$

The validity of the approximate form of Eq. (A17) is validated in the paper through the field tests of this study as well as other data from the literature.

As in Eq. (A2), the decay parameter K_{r0} is divided into two parts to describe the individual contribution of steady and unsteady friction to the transient envelope damping, as,

$$K_{r0} = K_{rs0} + K_{ru0} . \tag{A18}$$

Meanwhile, to better understand the impacts of system parameters and flow conditions on the importance of friction damping, the decay parameter K_{r0} in Eq. (A14) can be further simplified as conducted in Duan *et al.* (2012),

$$K_{r0} = K_{rs0} + K_{ru0} \approx \frac{f\boldsymbol{M}}{2}\frac{L}{D} + 8C_{\alpha\beta}\frac{\boldsymbol{M}}{\boldsymbol{Re}_0}\frac{L}{D} = \frac{f\boldsymbol{Re}_0}{2}\frac{T_w}{T_{dv}} + 8C_{\alpha\beta}\frac{T_w}{T_{dv}} , \tag{A19}$$

where $C_{\alpha\beta}$ is coefficient relating to α' and β' in Eq. (A7) for smooth case and Eq. (A8) for rough case, and applying $\omega^{*}\sim 1$ for the case of fast valve closure or sudden pump stoppage,

$$C_{\alpha\beta} = \alpha'\sqrt{\frac{\sqrt{1+(\beta')^2} - \beta'}{2\left[1+(\beta')^2\right]}} . \tag{A20}$$

Specifically, for the rough cases of the given single pipe in this study, it can be approximately obtained that,

$$C_{\alpha\beta} \approx 0.261\alpha'(\beta')^{-0.913}, \tag{A21}$$

with a fitness of this approximation to original Eq. (A20), $R^2 = 0.95$. As a result, for fully rough pipe flow case (e.g., the field tests of this study):

$$K_{r0} = K_{rs0} + K_{ru0} \approx \frac{f\boldsymbol{M}}{2}\frac{L}{D} + 0.024\left(\frac{\varepsilon}{D}\right)^{0.016}\left(\boldsymbol{M}\frac{L}{D}\right)^{-0.414} = \frac{f\boldsymbol{Re}_0}{2}\frac{T_w}{T_{dv}} + 0.024\left(\frac{\varepsilon}{D}\right)^{0.016}\left(\boldsymbol{Re}_0\frac{T_w}{T_{dv}}\right)^{-0.414} . \tag{A22}$$

Furthermore for clarity and completeness, the results for smooth pipe flow case summarized from Duan *et al.* (2012) are also shown here as,

$$K_{r0} = K_{rs0} + K_{ru0} \approx \begin{cases} \dfrac{f\boldsymbol{M}}{2}\dfrac{L}{D} + \sqrt{2\dfrac{L}{D}\dfrac{\boldsymbol{M}}{\mathrm{Re}_0}} & \text{if } \boldsymbol{M}\dfrac{L}{D} << 1 \\ \dfrac{f\boldsymbol{M}}{2}\dfrac{L}{D} + \dfrac{(\boldsymbol{Re}_0)^{0.063}}{30.33}\dfrac{D}{L}\dfrac{1}{M} & \text{otherwise} \end{cases}$$
$$= \begin{cases} \dfrac{f\boldsymbol{Re}_0}{2}\dfrac{T_w}{T_{dv}} + \sqrt{2\dfrac{T_w}{T_{dv}}} & \text{if } \boldsymbol{Re}_0\dfrac{T_w}{T_{dv}} << 1 \\ \dfrac{f\boldsymbol{Re}_0}{2}\dfrac{T_w}{T_{dv}} + \dfrac{1}{30.33(\boldsymbol{Re}_0)^{0.94}}\dfrac{T_{dv}}{T_w} & \text{otherwise} \end{cases} . \tag{A23}$$

It is necessary to note that Eqs. (A22) and (A23) are simplified for specific conditions such as the timescale ratio $\frac{T_w}{T_{dv}} << 1$ (Duan *et al.* 2012), and for obtaining general conclutions the original full version of Eqs. (A14) and (A15) should be used.

Table 1: Main characteristics of experimental tests

Test pipe system	Test no.	*L/D*	*f*	***M***	***Re***$_0$	Flow regime	***I***	K_{ru0}/K_{rs0}
Laboratory system (from Adamkowski and Lewandowski, 2006)	1	6132	0.036	0.00026	5731	*Smooth*	0.06	1.192
	2	6132	0.030	0.00049	10634	*Smooth*	0.09	0.431
	3	6132	0.027	0.00072	15843	*Smooth*	0.12	0.221
Field system tested by the authors of this study	4	16038	0.037	0.00031	97584	*Rough*	0.18	0.124
	5	16038	0.037	0.00043	136139	*Rough*	0.26	0.081
	6	16038	0.037	0.00076	239957	*Rough*	0.45	0.036
	7	16038	0.037	0.00124	386379	*Rough*	0.72	0.018

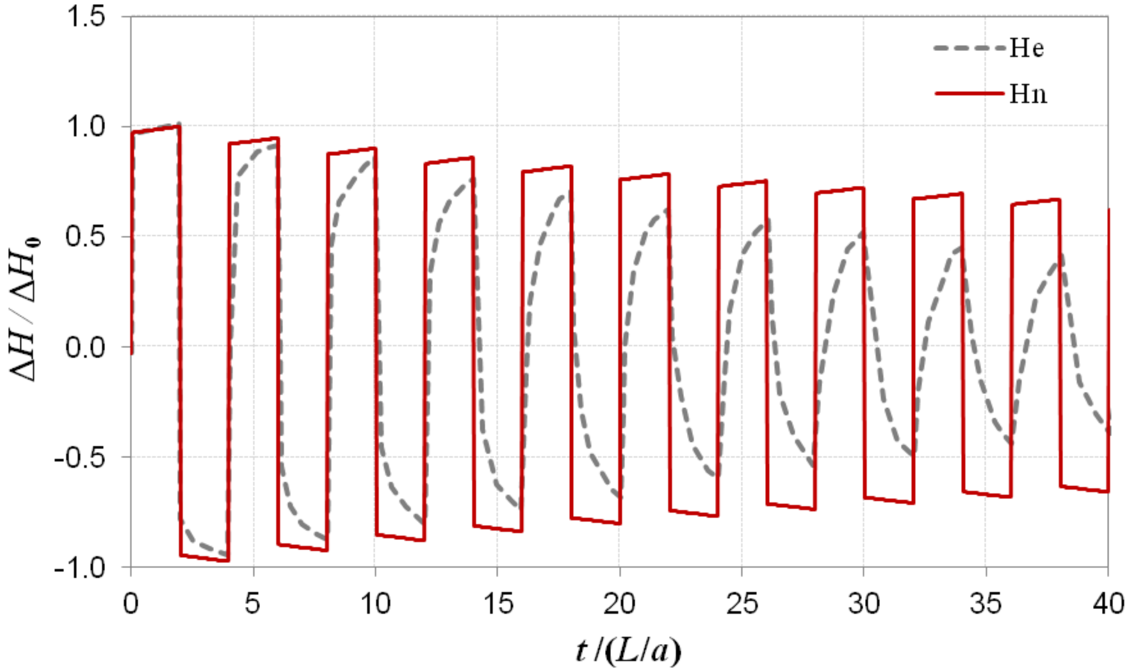

Figure 1: Experimental and numerical pressure signals for laboratory test with $\boldsymbol{Re}_0$ = 5731 (test no. 1 in Table 1; H_n is numerical result based on 1-D model, and H_e is experimental data retrieved from Adamkowski and Lewandowski, 2006)

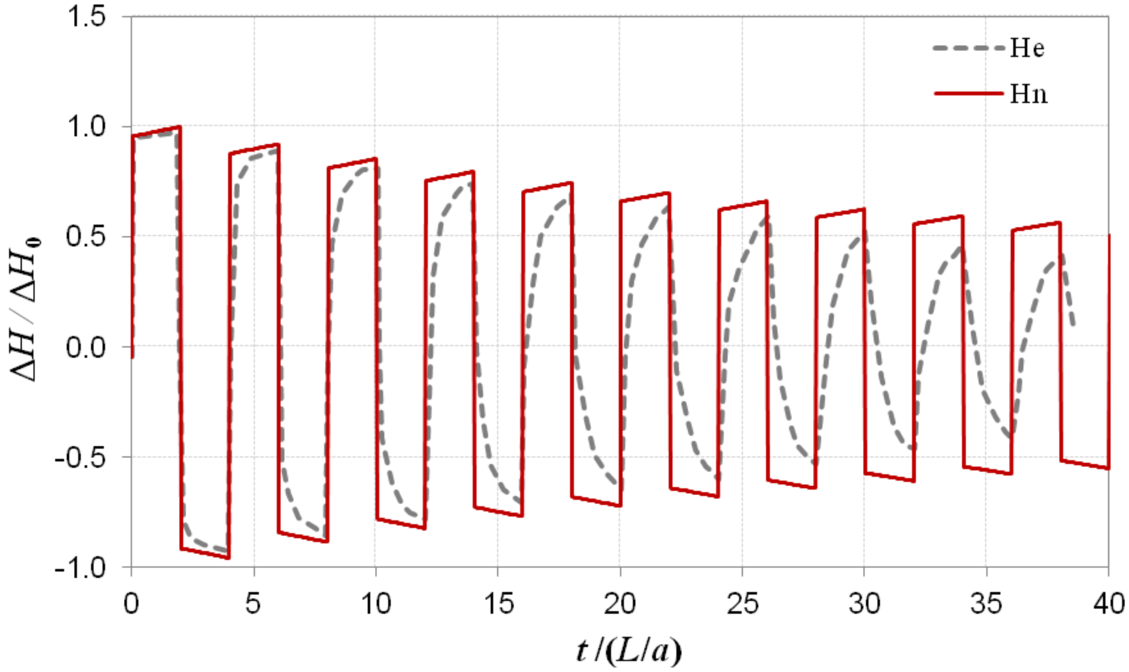

Figure 2: Experimental and numerical pressure signals for laboratory test with $\boldsymbol{Re}_0$ = 10634 (test no. 2 in Table 1; H_n is numerical result based on 1-D model, and H_e is experimental data retrieved from Adamkowski and Lewandowski, 2006)

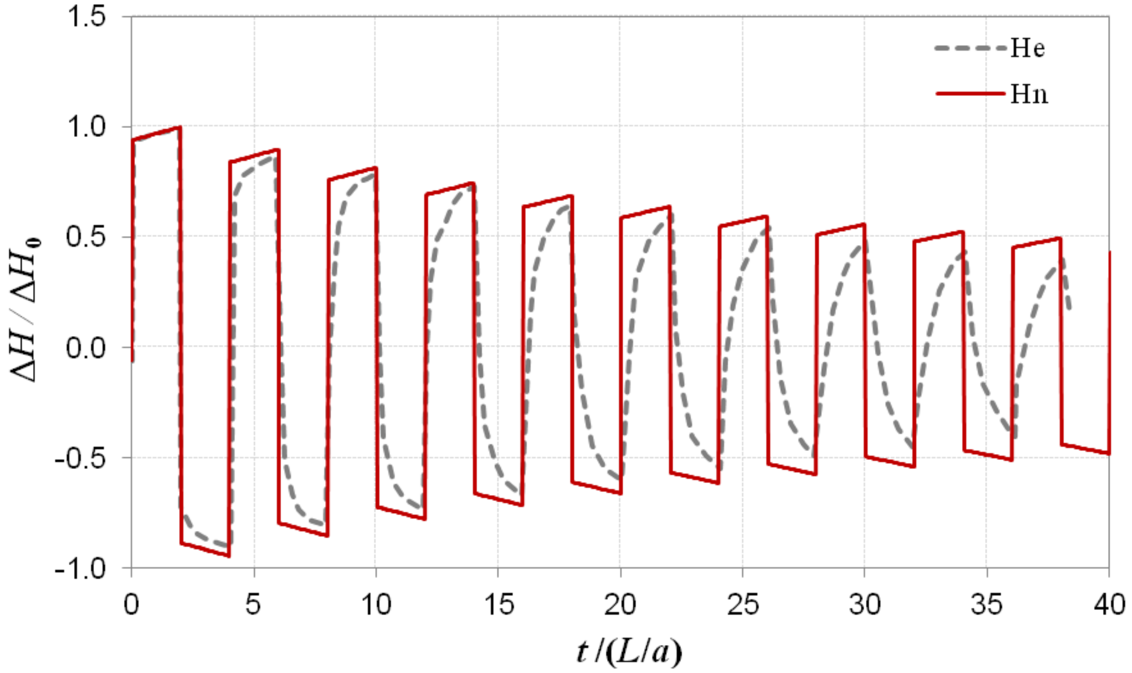

Figure 3: Experimental and numerical pressure signals for laboratory test with $\boldsymbol{Re}_0$ = 15843 (test no. 3 in Table 1; H_n is numerical result based on 1-D model, and H_e is experimental data retrieved from Adamkowski and Lewandowski, 2006)

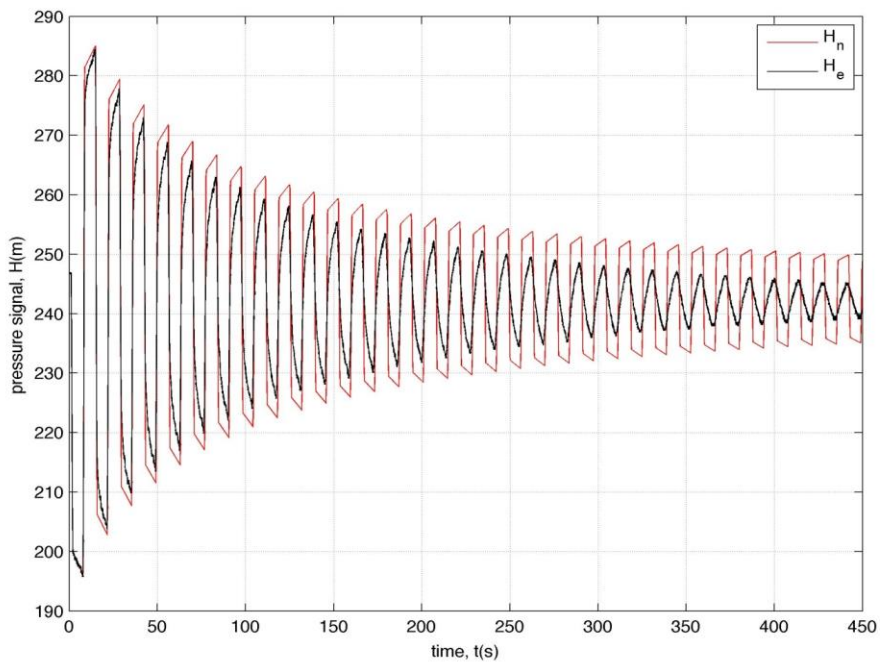

Figure 4: Experimental and numerical pressure signals for field test due to pump shutdown with $\boldsymbol{Re}_0$ = 97584 (test no. 4 in Table 1; H_n is numerical result based on 1-D model, and H_e is experimental data)

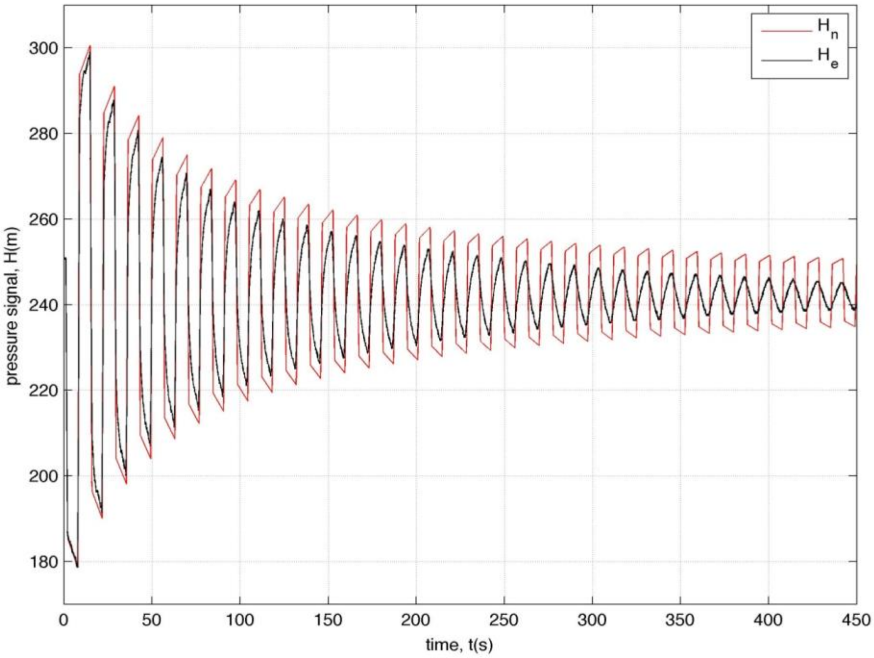

Figure 5: Experimental and numerical pressure signals for field test due to pump shutdown with $\boldsymbol{Re}_0$ = 136139 (test no. 5 in Table 1; H_n is numerical result based on 1-D model, and H_e is experimental data)

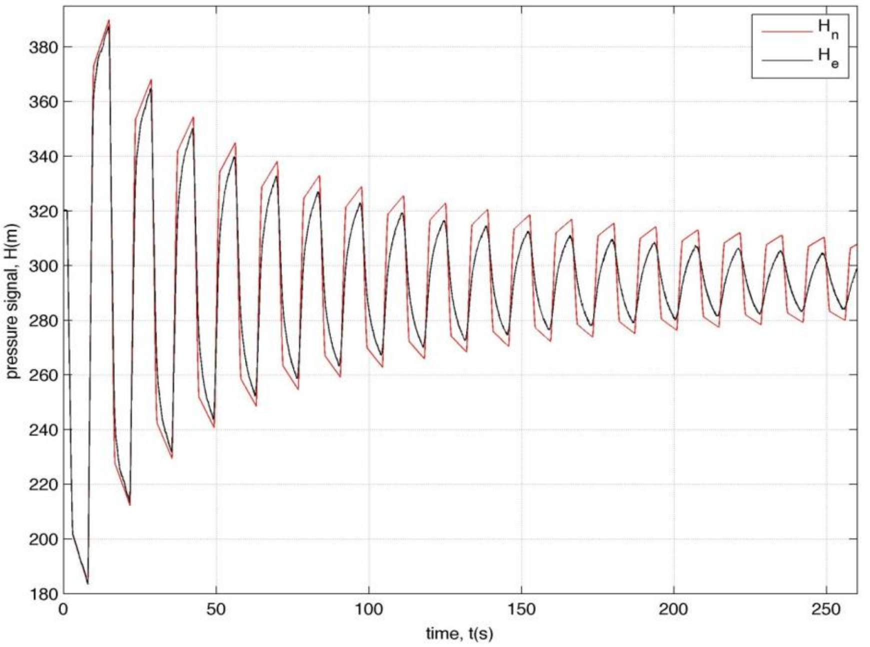

Figure 6: Experimental and numerical pressure signals for field test due to pump shutdown with $\boldsymbol{Re}_0$ = 239957 (test no. 6 in Table 1; H_n is numerical result based on 1-D model, and H_e is experimental data)

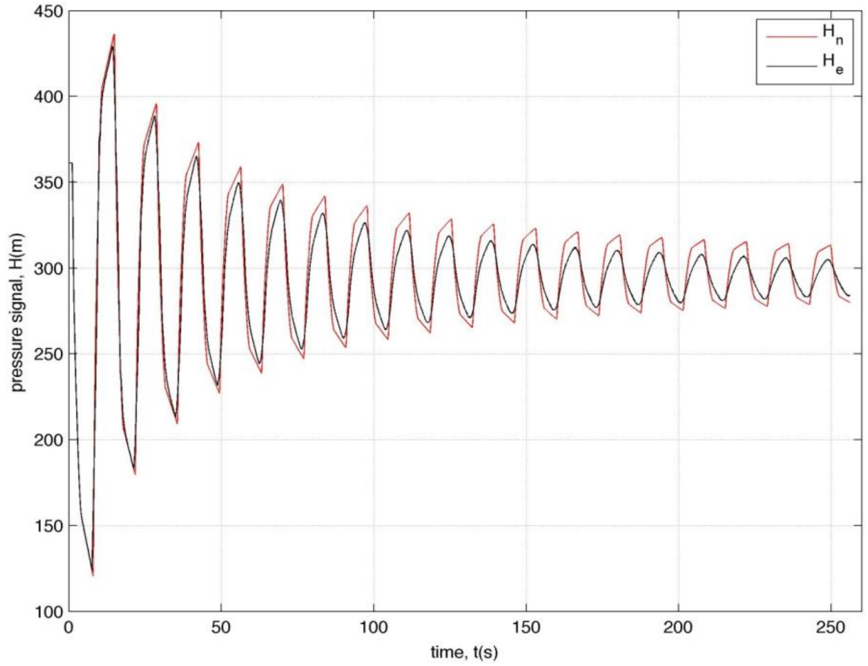

Figure 7: Experimental and numerical pressure signals for field test due to pump shutdown with $\boldsymbol{Re}_0$ = 386379 (test no. 7 in Table 1; H_n is numerical result based on 1-D model, and H_e is experimental data)

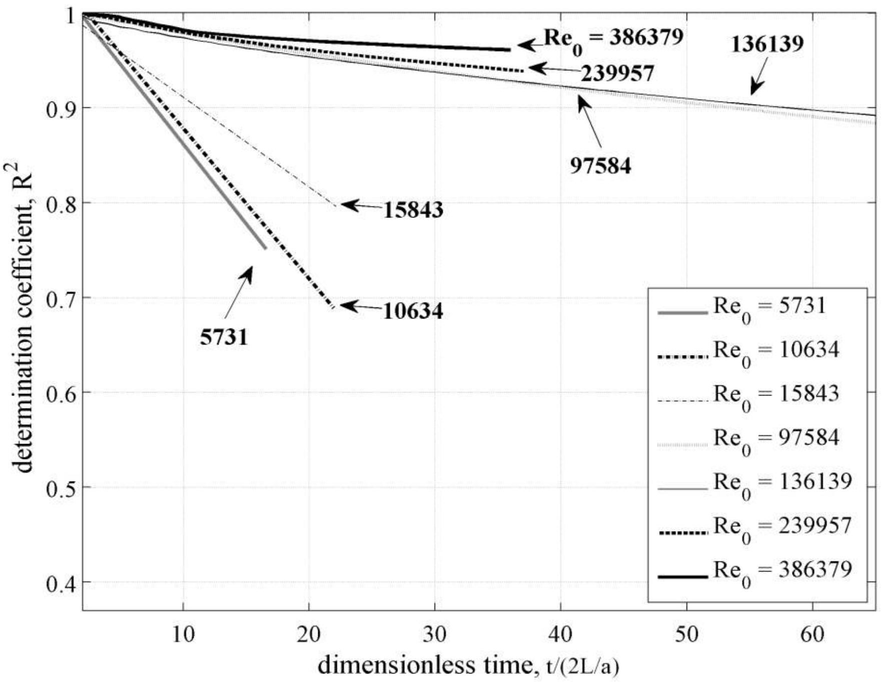

Figure 8: The determination coefficient, R^2, vs. the dimensionless time

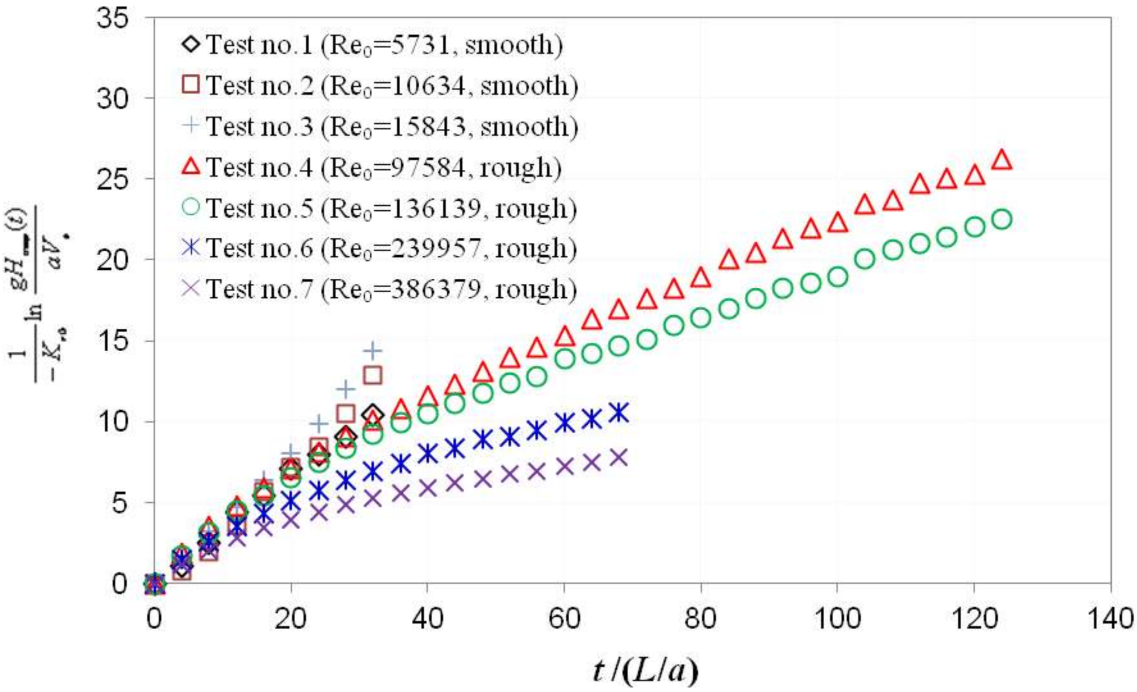

Figure 9: The variation of rescaled pressure amplitude with time using $\boldsymbol{Re}_0$ for test cases in Table 1

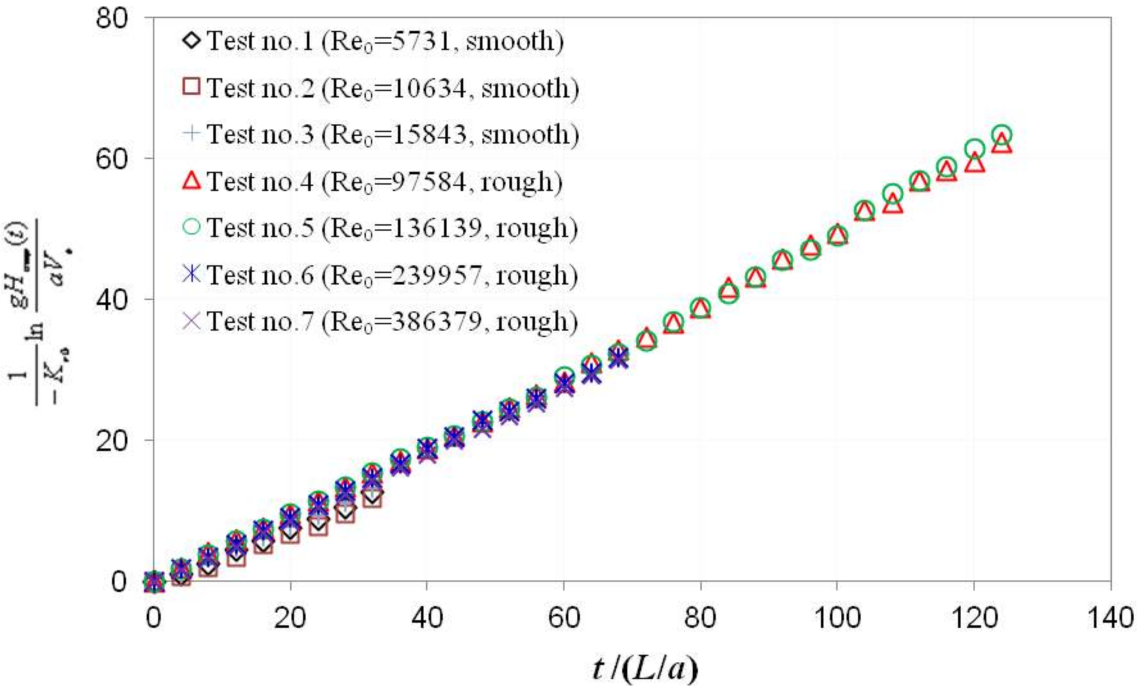

Figure 10: The variation of rescaled pressure amplitude with time using time dependent $\boldsymbol{Re}_t$ for test cases in Table 1

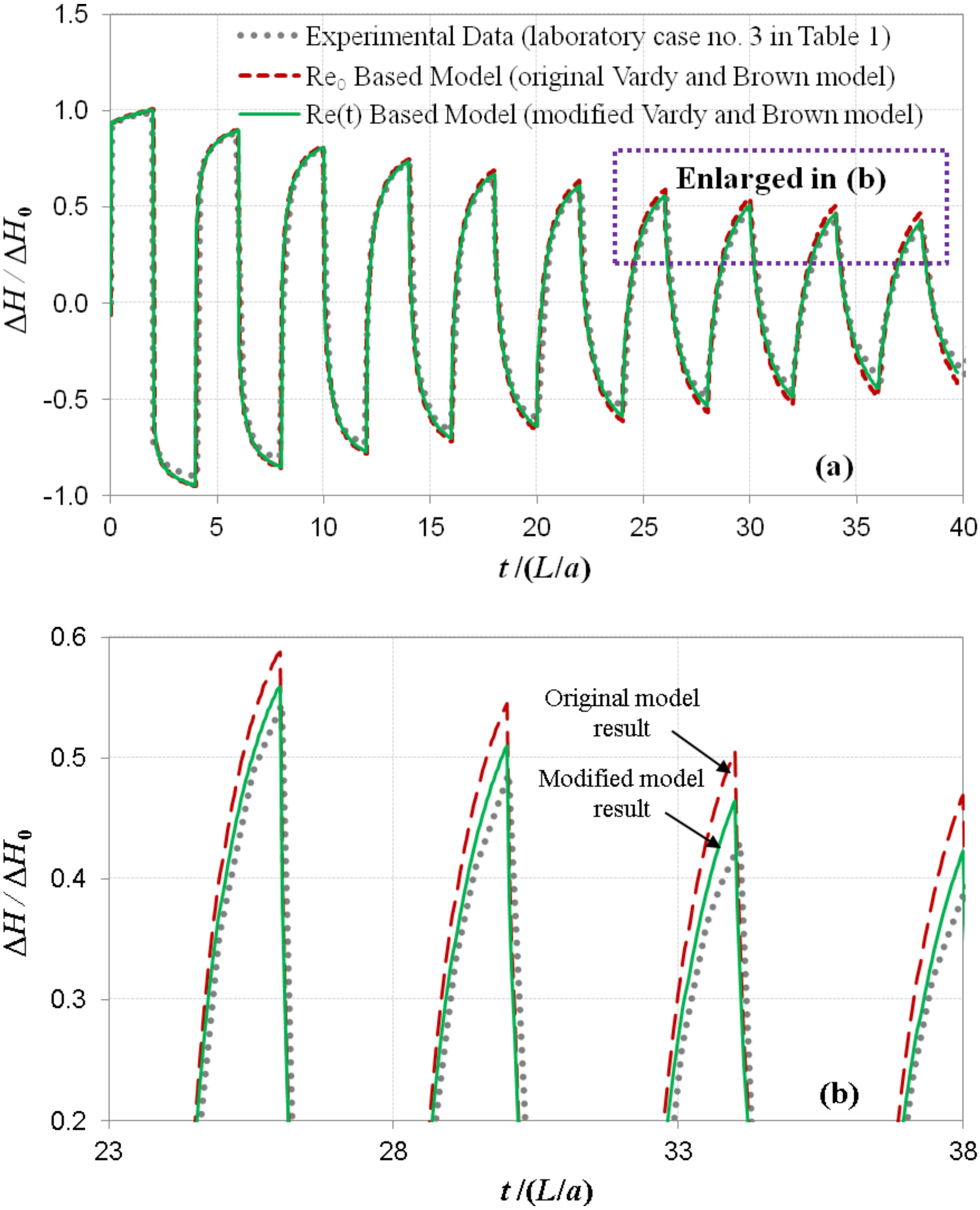

Figure 11: Experimental data and numerical results of pressure head traces based on different models for laboratory test case no. 3 in Table 1 ($\boldsymbol{Re}_0$=15843)

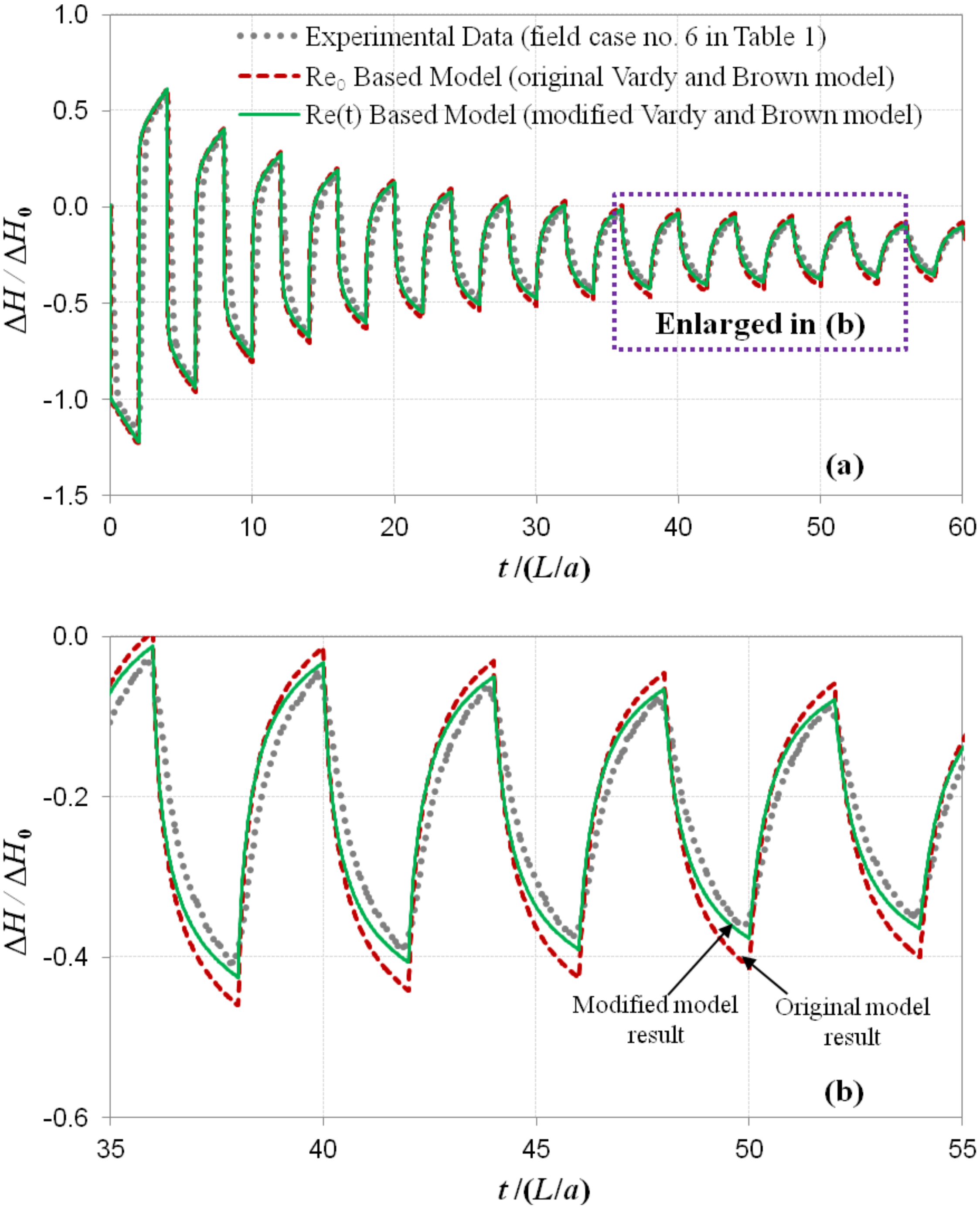

Figure 12: Experimental data and numerical results of pressure head traces based on different models for field test case no. 6 in Table 1 ($\boldsymbol{Re}_0$=239957)